

Direct Microstability Optimization of Stellarator Devices

R. Jorge,¹ W. Dorland,^{2,3,4} P. Kim,² M. Landreman,³ N. R. Mandell,⁴ G. Merlo,⁵ and T. Qian⁴

¹*Instituto de Plasmas e Fusão Nuclear, Instituto Superior Técnico,
Universidade de Lisboa, 1049-001 Lisboa, Portugal**

²*Department of Physics, University of Maryland, College Park, MD 20742, USA*

³*Institute for Research in Electronics and Applied Physics,
University of Maryland, College Park, MD 20742, USA*

⁴*Princeton Plasma Physics Laboratory, Princeton, NJ 08543, USA*

⁵*Oden Institute for Computational Engineering and Sciences,
The University of Texas at Austin, Austin, TX 78712, United States of America*

Turbulent transport is regarded as one of the key issues in magnetic confinement nuclear fusion, both for tokamaks in stellarators. In this letter, we show that a significant decrease in the turbulent heat flux can be obtained in an efficient manner by coupling stellarator optimization with linear gyrokinetic simulations. This is accomplished by computing the quasi-linear heat flux at each step of the optimization process, as well as the deviation from quasisymmetry, and minimizing their sum, leading to a balance between neoclassical and turbulent transport.

Introduction.— The stellarator is a class of fusion devices that can run in a steady state due to the flexible shaping of the confining magnetic field and the absence of current-driven instabilities [1]. This inherent flexibility allows stellarators to be optimized for a wide range of parameters, with W7-X [2] and HSX [3] examples of the experimental realizations of such optimization studies. One of the main difficulties in stellarator optimization is the balance between neoclassical transport, driven by trapped particles in a low collisionality regime, and turbulent transport in the core, the latter being driven largely by microinstabilities [4]. As an example, while W7-X has successfully shown decreased neoclassical transport, as in the tokamak case, turbulent transport is still limiting its energy confinement time [5]. Indeed, turbulent transport is currently one of the main limiting factors in the performance of magnetic confinement fusion devices. Although we are currently able to predict turbulent transport in the core with relative accuracy, we still need an effective way to design machines with low turbulent transport, specifically, microinstability-driven turbulent transport [4, 6].

In this Letter, we directly target both (1) the reduction of the microinstability drive of turbulent transport, and (2) the trapped particle losses driving neoclassical transport. As we show here, depending on the weights used, a balance between the two types of transport is possible, and magnetic field equilibria with enhanced confinement properties can be achieved. While previous optimization methods targeted cost functions based on proxy functions relying solely on the properties of the magnetic field equilibrium [7–9], here, we do not rely on proxy functions to evaluate microstability and directly solve the gyrokinetic equation at each iteration. To our knowledge, this is the first study where gyrokinetic calculations are performed within the optimization at every iteration. We note that, while in this study a particular numerical tool is used to solve the gyrokinetic equation and extract its

linear growth rates and eigenfunctions, the direct optimization method employed here can be applied to other equilibrium and gyrokinetic codes which model different instability types and can easily be generalized to directly optimize turbulent heat and particle fluxes.

The framework used in this work to assess microstability is gyrokinetics. This is considered to be one of the main tools to assess the stability of fusion devices at spatial scales on the order of, or smaller than, the ion gyroradius ρ_i and at frequencies lower than the ion gyrofrequency Ω_i [10–12] and is usually regarded as the most complete, yet numerically efficient, framework to treat strongly magnetized plasmas [13]. For this reason, we quantify instabilities in this work by solving the linearized gyrokinetic equation to obtain the growth rates and corresponding eigenfunctions associated with the underlying instabilities. The instability studied here is the ion-temperature-gradient (ITG) mode, which is commonly regarded as one of the most transport-relevant electrostatic instabilities in tokamaks and stellarators [14, 15].

The ITG mode develops on the ion gyroscale and is widely recognized as one of the main candidates to explain the experimental observations of anomalous ion heat turbulent transport in the core of fusion devices [16] as corroborated by numerical simulations [17–19]. The study of solely ion-driven instabilities such as the ITG mode is performed by removing the fast electron dynamics induced by electron inertia, meaning that the electron density in our model follows the perturbed electrostatic potential ϕ via the Boltzmann response. The ITG mode can also deteriorate plasma confinement in electron heating scenarios by creating ion temperature clamping, preventing the heating of ions in the plasma core above 2 keV [20]. While ITG can drive a certain amount of electron heat flux (usually proportional to the driven ion heat flux), contributions to the electron heat flux from trapped electron modes are expected if the ITG

is not sufficient to drive the electron heat flux imposed by the applied heating power [21].

As an optimization criterion to stabilize the underlying unstable modes, we choose our objective function J to be a quasi-linear estimate [4, 22] for the heat flux f_Q with the growth rates γ and associated eigenfunctions calculated using linear gyrokinetic simulations. The method employed here can also be used with nonlinear gyrokinetic or fluid codes by replacing the quasi-linear estimate f_Q with the nonlinear heat flux Q computed by the respective code. This differs from previous objective functions that also targeted the reduction of turbulent transport such as Refs. [7, 9, 23] as these are solely based on properties of the equilibrium magnetic field, therefore requiring more assumptions about the geometry and the underlying modes. We note that, while the peak growth rate γ could be chosen as the objective function, we found it not to be a reliable indicator of the nonlinear heat flux due to the importance of smaller wave numbers. The reduction of neoclassical transport is performed by targeting quasisymmetry, an invariance of the magnetic field strength B that guarantees confinement of the collisionless trajectories up to a threshold energy [24]. As shown in Ref. [25], it is indeed possible to design stellarators with precise quasisymmetry and achieve unprecedented levels of collisionless particle confinement and collisional transport for a thermal plasma. We leverage such findings by adding to the objective function J the term f_{QS} defined in Eq. (1) of Ref. [25] as it is already in a form ready to be used in a least squares optimization method and, unlike previous optimization metrics, it does not require the calculation of Boozer coordinates [26] at each optimization step.

Method.— The growth rates γ are calculated using the GS2 code [27–29] that solves the gyrokinetic equation

$$\frac{dh}{dt} + v_{\parallel} \mathbf{b} \cdot \nabla h + \mathbf{v}_d \cdot \nabla h = C + \frac{qF_0}{T_0} \frac{\partial \chi}{\partial t}, \quad (1)$$

coupled with the quasineutrality condition and Ampère’s law. In Eq. (1), F_0 is the equilibrium distribution function, $h = f - F_0(1 - q\phi/T_0)$ is the non-adiabatic part of the distribution function f , $\chi = \langle \phi - \mathbf{v} \cdot \mathbf{A}/c \rangle$ is the gyroaveraged gyrokinetic potential with ϕ the electrostatic potential and \mathbf{A} the magnetic vector potential, $d_t = \partial_t + (c/B)[\chi, \cdot]$ is the total time derivative with $[\chi, h] = \partial\chi/\partial\mathbf{R} \times \partial h/\partial\mathbf{R} \cdot \mathbf{b}$ the Poisson bracket, $\mathbf{v}_d = (\mathbf{b}/2\Omega_0) \times (2v_{\parallel}^2 \mathbf{b} \cdot \nabla \mathbf{b} + v_{\perp}^2 \nabla B_0/B_0)$ is the drift velocity with B_0 the equilibrium magnetic field, $\Omega_0 = qB_0/m$ is the gyrofrequency with q the particle’s charge and m its mass, and C is the gyroaveraged collision operator. To focus on ITG modes, we reduce the gyrokinetic equation to its linear electrostatic flux-tube limit employing the adiabatic electron approximation, solve it as an initial value problem, and fit the temporal evolution of the absolute value of the electrostatic potential to an exponential of the form $\exp(\gamma t)$ with γ the growth rate.

At the end of the optimization, we assess the level of turbulent transport of each configuration by solving the nonlinear gyrokinetic system of equations, Eq. (1), using GX [30, 31], a code that natively targets graphics processor units (GPUs) and uses a pseudospectral decomposition in velocity space to enable efficient nonlinear calculations. While GX can also solve the linear gyrokinetic equation to obtain the corresponding growth rates, the GS2 code employs a more numerically efficient implicit initial-value algorithm for obtaining the linear microstability growth rates on a wavenumber-by-wavenumber basis, and is therefore the code used during the optimization procedure.

The GS2 and GX codes employ a Fourier decomposition of the physical quantities in the x (normal) and y (binormal) directions with $\mathbf{k}_{\perp} = k_x \nabla x + k_y \nabla y$ the perpendicular wave-vector and $\mathbf{r} = (x, y, z)$ the spatial coordinates. Such coordinates are based on the Clebsch representation for the equilibrium magnetic field $\mathbf{B} = \nabla\psi \times \nabla\alpha$ with ψ the toroidal magnetic flux and α a field line label on the flux surface. The coordinates are then defined as $x = a\sqrt{s}$ with a a reference length taken here as the effective minor radius of the stellarator (see definition in page 12 of Ref. [32]) and $s = \psi/\psi_b$ where ψ_b is the value of ψ at the outermost flux surface (otherwise known as plasma boundary), $y = x\alpha$ and z a dimensionless coordinate along the field line.

The density and temperature profiles are assumed to decay exponentially in x with a constant scale length $L_n/a = -d \ln n/dx$ and $L_T/a = -d \ln T/dx$, respectively. For this work, we simulate flux tubes with $s = 0.25$ and linearly evolve modes with $k_x = \alpha = 0$ with a grid of ten values of $0.3 \leq k_y \leq 3.0$. However, we note that while the choice $\alpha = 0$ is expected to lead to a peak of the modes mainly on the outboard side [19] where the choice $k_x = 0$ is likely to yield growth rates at or close to the maximum one, this hypothesis is corroborated *a posteriori* via the nonlinear simulations with GX at finite k_y and k_x . The density and temperature profiles used are $a/L_n = 1$ and $a/L_T = 3$, respectively, with a the minor radius, leading to $\eta = L_T/L_n = 3$, a typically used value in cyclone base case scenarios [33]. The remaining input parameters for GS2 were obtained by performing convergence tests for the initial and final equilibria of each optimization in a similar fashion to Ref. [34].

We then write the quasi-linear estimate f_Q for the heat flux using a mixing length saturation rule [35]

$$f_Q = \sum_{k_y} \frac{\gamma(k_y)}{\langle k_{\perp}^2 \rangle (k_y)}, \quad (2)$$

where the sum is taken over all values of k_y used in the simulation, and $\langle k_{\perp}^2 \rangle = \int g^{yy} k_y^2 |\hat{\phi}|^2 \sqrt{g} dz / \int |\hat{\phi}|^2 \sqrt{g} dz$ is the flux-surface average of the squared perpendicular wave number with $|\hat{\phi}|$ the amplitude of the mode and \sqrt{g} the Jacobian. As shown in [4], such quasi-linear transport

model overcomes some of the limitations of the heuristic mixing length estimate γ/k_y^2 by taking into account the extension of the toroidal modes along z .

The components of the magnetic field equilibrium relevant to compute both the geometric coefficients entering Eq. (1) and the quasisymmetry objective function f_{QS} are calculated using the Variational Moments Equilibrium Code (VMEC) [36]. VMEC finds a solution of ideal magnetohydrodynamics (MHD) equation $\mathbf{J} \times \mathbf{B} = \nabla P$, with $\mathbf{J} = \nabla \times \mathbf{B}/\mu_0$ the plasma current and P the plasma pressure, by applying a variational method to the integral form of the MHD equations. We run VMEC in fixed-boundary mode where an MHD equilibrium is obtained by specifying the last closed flux surface S as boundary condition parametrized by two variables (θ, ϕ) , namely an angle-like variable termed the poloidal angle θ and the standard cylindrical toroidal angle ϕ , respectively, allowing us to define $S = [R(\theta, \phi) \cos(\phi), R(\theta, \phi) \sin(\phi), Z(\theta, \phi)]$ where $R = \sum_{m=0}^{M_{\text{pol}}} \sum_{n=-N_{\text{tor}}}^{N_{\text{tor}}} \text{RBC}_{m,n} \cos(m\theta - n_{\text{fp}}n\phi)$ and $Z = \sum_{m=0}^{M_{\text{pol}}} \sum_{n=-N_{\text{tor}}}^{N_{\text{tor}}} \text{ZBS}_{m,n} \sin(m\theta - n_{\text{fp}}n\phi)$. In the Fourier decompositions of R and Z , the sin and cos terms are set to zero, respectively, to ensure stellarator-symmetry [37] and n_{fp} is the toroidal periodicity of the equilibrium. While stellarator symmetry is, in principle, not necessary, it allows us to restrict the total number of degrees of freedom while still providing adequate optimized solutions. Given a plasma boundary S , a plasma pressure profile $P(\psi)$, and a net toroidal current I , VMEC seeks a solution of the ideal MHD system of equations with nested closed flux surfaces.

The optimization algorithm, the calculation of the quasisymmetry objective function, and the calculation of the geometric coefficients that enter the gyrokinetic equation are performed using the SIMSOPT code [38]. The independent variables for optimization are the boundary Fourier coefficients $\{\text{RBC}_{m,n}, \text{ZBS}_{m,n}\}$ excluding $\text{RBC}_{0,0}$ which is set to one to fix the spatial scale. We use as initial condition the precise quasi-helically (QH) symmetric configuration of Ref. [25] with $n_{\text{fp}} = 4$ and set to zero all surface modes with $m \geq 2$ and $|n| \geq 2$. Finally, in order to keep the same aspect ratio as the provided initial condition to the optimization, we add to the objective function J the term $f_A = (A - A^*)^2$ where A is the aspect ratio of the configuration computed at each iteration and $A^* = 8$ the target (initial) aspect ratio. The final objective function is then given by

$$J = \omega_{f_Q} f_Q + f_{QS} + f_A, \quad (3)$$

where ω_{f_Q} is the weight given to the minimization of f_Q .

Results.— We first perform a parameter space scan to guide the choice of our optimization algorithm. Namely, we assess the dependence of the quasisymmetry cost function f_{QS} and the quasi-linear estimate f_Q on the geometry of the magnetic field by performing a scan on the

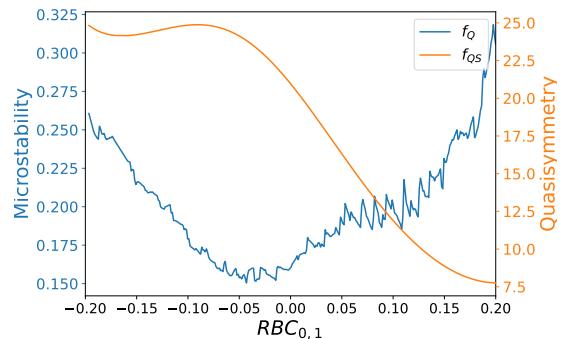


FIG. 1. Quasi-linear estimate f_Q and quasisymmetry cost function f_{QS} as a function of the surface shape parameter $\text{RBC}_{0,1}$ for the quasi-helically symmetric configuration used as initial conditions for the optimization.

$\text{RBC}_{0,1}$ boundary mode in the range $(-0.2, 0.2)$ on the initial precise QH configuration where $\text{RBC}_{0,1} = 0.180$. This is shown in Fig. 1 with the value of f_Q illustrating microstability in blue and the value of f_{QS} illustrating quasisymmetry in orange. We find that while there are only two local minima of f_{QS} , the cost function f_Q contains many local minima with its global minimum at a different location than the global minimum of f_{QS} . Therefore, when performing optimization studies on both quasisymmetry and microstability, a compromise on the level of quasisymmetry is expected. Given the fact that the local minima of f_Q and f_{QS} appear to be well separated, and that the roughness of the cost function f_Q does not lead to large jumps in f_Q for small changes of $\text{RBC}_{0,1}$, we use a local optimization algorithm instead of a global optimization algorithm. This leads to a more efficient optimization method but it may not result in the global minimum of the objective function found. However, as it is shown below, the solution found is able to fulfill our desired criteria. The optimization is carried out using the python library scipy [39] for nonlinear least-squares minimization by employing the Levenberg-Marquardt method. Gradients are computed using finite differences, with MPI for concurrent function evaluations where, at each iteration, both the magnetic field inside the boundary (using VMEC) and the gyrokinetic simulations (using GS2) are computed within the SIMSOPT framework. In order to steer the optimizer away from the many local minima present in f_Q and still be able to use finite differences, we use a large value for the relative Δ_r and absolute Δ_a step sizes ($\Delta_r = 0.1$ and $\Delta_a = 0.01$) and perform an extra optimization to refine the minimum found by decreasing the relative step size to $\Delta_r = 0.01$. We note that the study in Fig. 1 is performed by varying a single parameter and the extrapolation of such findings to other optimization parameters would need a multi-dimensional survey. Therefore, an *a posteriori* examination of the growth rates and nonlinear fluxes is performed to assess the effectiveness of this optimization procedure.

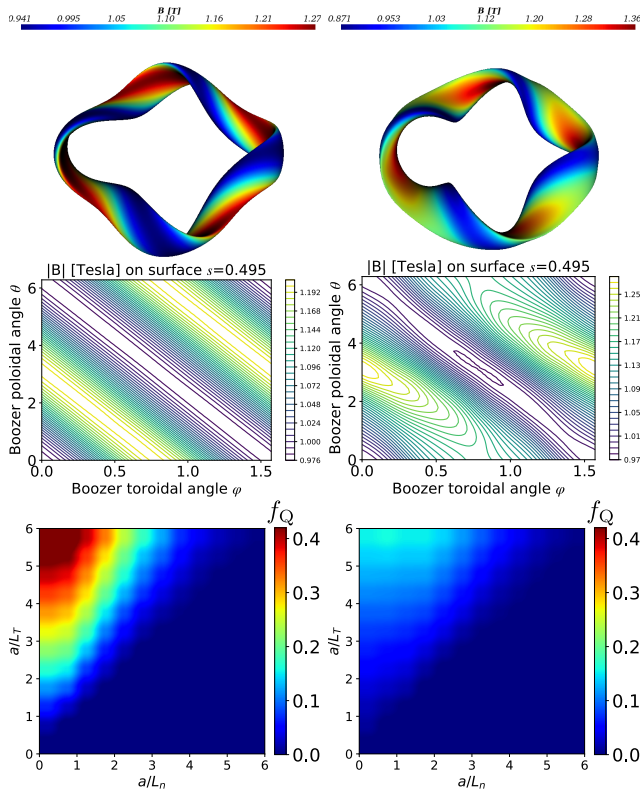


FIG. 2. Top: Magnetic field configuration optimized for quasisymmetry with $\omega_{f_Q} = 0$ (left) and the configuration optimized for quasisymmetry and microstability with $\omega_{f_Q} = 10$ (right) where the color shows the magnetic field strength on that surface. Middle: Field strength on an $s = 0.495$ flux surface in Boozer coordinates for $\omega_{f_Q} = 0$ (left) and $\omega_{f_Q} = 10$ (right). Bottom: Comparison of the quasi-linear estimate for the heat flux between the configuration optimized for $\omega_{f_Q} = 0$ (left) and $\omega_{f_Q} = 10$ (right) for several profile scale lengths L_n and L_T .

We perform two optimization studies. The first targets only quasisymmetry by setting $\omega_{f_Q} = 0$ and will be used as a benchmark case. The resulting optimization is shown in Fig. 2 (left). The second targets both microstability and quasisymmetry simultaneously and sets $\omega_{f_Q} = 10$. We find that values of ω_{f_Q} higher than 10 do not lead to a significant decrease in f_Q but instead result in increased values of f_{QS} , while values smaller than 10 lead to increased values of f_Q . The resulting optimization is shown in Fig. 2 (right). The overall optimization was done in an iterative fashion, namely, an optimization with large and smaller step sizes was performed at each of maximum surface Fourier modes $M_{\text{pol}} = N_{\text{tor}} = 1, 2, 3$. A further increase of M_{pol} and N_{tor} resulted in negligible improvements in the objective function in the $\omega_{f_Q} = 10$ case. Therefore, the resulting configurations have only surface Fourier modes up to $m \leq 3$ and $|n| \leq 3$. We find that, in the first case, f_{QS} was reduced to 1.14×10^{-4} with $f_Q = 12.9 \times 10^{-2}$, while in the second case f_Q was reduced

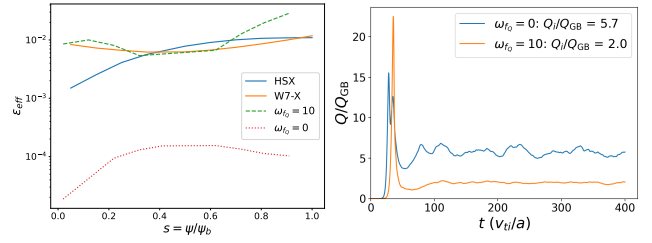


FIG. 3. Left: Relative levels of neoclassical transport for a thermal plasma in the $1/\nu$ regime, measured using the effective helical ripple quantity ϵ_{eff} , between the configurations found in this work and two of the most recently built stellarators, the quasi-helical symmetric HSX machine and the quasi-isodynamic W7-X machine. Right: Time traces (in units of the ion thermal velocity, v_{ti} over the minor radius, a) of the nonlinear ion heat flux Q_i , normalized to gyro-Bohm units, Q_{GB} , for both the magnetic field configuration optimized for quasisymmetry with $\omega_{f_Q} = 0$ (blue) and the configuration optimized for quasisymmetry and microstability with $\omega_{f_Q} = 10$ (orange) where a $\sim 65\%$ reduction in Q_i/Q_{GB} is found.

to 5.94×10^{-2} with $f_{QS} = 8.86 \times 10^{-2}$. In order to assess the deterioration in quasisymmetry, we show in Fig. 2 (middle) the contours of the magnetic field strength at $s = 0.495$ with the deviation from straight lines appearing in the second case (optimization for microstability). On the other hand, the enhanced microstability properties of the resulting configuration is evident even at values of L_n and L_T outside the ones used for the optimization, see Fig. 2 (bottom).

We now perform an *a posteriori* assessment of the neoclassical and turbulent transport of the optimized configurations. As a metric for neoclassical transport, we use the magnitude of the collisional transport for a thermal plasma in the $1/\nu$ regime (with ν the collision frequency), also known as the effective helical ripple ϵ_{eff} . This quantity is computed using the NEO code [40]. In Fig. 3 (left) we show the value of ϵ_{eff} for both the quasisymmetry only configuration ($\omega_{f_Q} = 0$) and the quasisymmetry and microstability optimized configuration ($\omega_{f_Q} = 10$). We see that while the first case leads to lower values of ϵ_{eff} , the values of ϵ_{eff} for the microstability optimized case are within the range of current optimized experiments such as the HSX [3] and W7-X [41] devices. Regarding fast particle confinement, we assess the fraction of lost particles to the surface by tracing the guiding center motion of 5000 test particles initialized isotropically on the $s = 0.25$ surface followed using the SIMPLE code [42] for 0.2s. For this case, the configurations are scaled to the same minor radius 1.7m and field strength on-axis of $B_0 = 5.7\text{T}$ of the ARIES-CS fusion reactor study, in a similar fashion as in [25, 43]. We find that the quasisymmetry optimization leads to no loss of particles, while the microstability optimized case leads to a loss fraction of $\sim 5\%$ at 0.2s.

Finally, we verify whether the increased microstability of the $\omega_{f_Q} = 10$ optimized configuration leads to

a decrease in turbulent transport. We show in Fig. 3 (right) the ion heat flux Q_i normalized to gyro-Bohm units from a nonlinear gyrokinetic simulation obtained using the GX code. Indeed, we find that the microstability optimized configuration leads to a $\sim 65\%$ reduction in the ion heat flux Q with respect to the configuration optimized only for quasisymmetry. These calculations used a resolution of 16 and 8 spectral modes in parallel and perpendicular velocity space, respectively, 192 grid points in x and 128 grid points in y (corresponding to $N_{k_x} = 127$ and $N_{k_y} = 43$ de-aliased Fourier modes, respectively), 250 grid points in z and a perpendicular box size of $75\rho_i \times 75\rho_i$, with ρ_i the ion Larmor radius.

Conclusions.— In this Letter, for the first time, microstability is taken into account in the optimization of quasisymmetric magnetic field configurations using first-principles gyrokinetic simulations. We were able to significantly reduce the quasi-linear estimate for the heat flux, leading to a smaller nonlinear heat flux, although at the cost of larger neoclassical transport. Notwithstanding, the resulting fast particle loss is still smaller than most stellarator designs to date and with similar levels of neoclassical transport. An extension of the framework introduced here to directly optimize for turbulent transport by replacing a quasi-linear estimate for the heat flux with its nonlinear counterpart linear gyrokinetic simulations in the optimization by nonlinear ones will be the subject of future work.

Data Availability.— The data supporting this study's findings are available in Zenodo at <https://doi.org/10.5281/zenodo.7415457>.

Acknowledgements.— We thank A. Goodman for fruitful discussions as well as the GS2, GX, and SIMSOPT teams for their invaluable contributions. This work has been carried out within the framework of the EUROfusion Consortium, funded by the European Union via the Euratom Research and Training Programme (Grant Agreement No 101052200 — EUROfusion). IST activities also received financial support from FCT - Fundação para a Ciência e Tecnologia through projects UIDB/50010/2020 and UIDP/50010/2020. R. J. is supported by FCT grant number 2021.02213.CEECIND. N.R.M. was supported by the US DOE Fusion Energy Sciences Postdoctoral Research Program administered by the Oak Ridge Institute for Science and Education (ORISE) for the DOE via Oak Ridge Associated Universities (ORAU) under DOE contract number DE-SC0014664. T.Q. is supported by the NSF Graduate Research Fellowship Program grant number DGE-2039656. The optimization studies were carried out using the EUROfusion Marconi supercomputer facility. Views and opinions expressed here are those of the author(s) only and do not necessarily reflect those of the European Union, the European Commission, DOE, NSF, ORAU, or ORISE. None of these parties can be held responsible for them.

* rogerio.jorge@tecnico.ulisboa.pt

- [1] P. Helander. Theory of plasma confinement in non-axisymmetric magnetic fields. *Reports on Progress in Physics*, 77(8):087001, 2014.
- [2] J. Geiger, C. D. Beidler, Y. Feng, H. Maassberg, N. B. Marushchenko, et al. Physics in the magnetic configuration space of W7-X. *Plasma Physics and Controlled Fusion*, 57(1):014004, 2015.
- [3] F. S. B. Anderson, A. F. Almagri, D. T. Anderson, P. G. Matthews, J. N. Talmadge, et al. The Helically Symmetric Experiment, (HSX) Goals, Design and Status. *Fusion Technology*, 27(3T):273, 1995.
- [4] F. Jenko, T. Dannert, and C. Angioni. Heat and particle transport in a tokamak: advances in nonlinear gyrokinetics. *Plasma Physics and Controlled Fusion*, 47(12B):B195, 2005.
- [5] C. D. Beidler, H. M. Smith, A. Alonso, T. Andreeva, J. Baldzuhn, et al. Demonstration of reduced neoclassical energy transport in Wendelstein 7-X. *Nature* 2021 596:7871, 596(7871):221–226, 2021.
- [6] C. Holland, L. Schmitz, T. L. Rhodes, W. A. Peebles, J. C. Hillesheim, et al. Advances in validating gyrokinetic turbulence models against L- and H-mode plasmas a). *Physics of Plasmas*, 18(5):056113, 2011.
- [7] H. E. Mynick, N. Pomphrey, and P. Xanthopoulos. Optimizing stellarators for turbulent transport. *Physical Review Letters*, 105(9):095004, 2010.
- [8] P. Xanthopoulos, H. E. Mynick, P. Helander, Y. Turkin, G. G. Plunk, et al. Controlling turbulence in present and future stellarators. *Physical Review Letters*, 113(15):155001, 2014.
- [9] G. T. Roberg-Clark, P. Xanthopoulos, and G. G. Plunk. Reduction of electrostatic turbulence in a quasi-helically symmetric stellarator via critical gradient optimization. *arXiv preprint*, arXiv:2210, 2022.
- [10] P. J. Catto. Linearized gyro-kinetics. *Plasma Physics*, 20(7):719, 1978.
- [11] T. M. Antonsen and B. Lane. Kinetic equations for low frequency instabilities in inhomogeneous plasmas. *The Physics of Fluids*, 23(6):1205, 1980.
- [12] E. A. Frieman, G. Rewoldt, W. M. Tang, and A. H. Glasser. General theory of kinetic ballooning modes. *Physics of Fluids*, 23(9):1750, 1980.
- [13] P. Helander and G. G. Plunk. Upper Bounds on Gyrokinetic Instabilities in Magnetized Plasmas. *Physical Review Letters*, 127(15):155001, 2021.
- [14] W. Horton. Drift waves and transport. *Reviews of Modern Physics*, 71(3):735, 1999.
- [15] P. Helander, J. H.E. Proll, and G. G. Plunk. Collisionless microinstabilities in stellarators. I. Analytical theory of trapped-particle modes. *Physics of Plasmas*, 20(12), 2013.
- [16] X. Garbet, P. Mantica, C. Angioni, E. Asp, Y. Baranov, et al. Physics of transport in tokamaks. *Plasma Physics and Controlled Fusion*, 46(12B):B557, 2004.
- [17] T. S. Hahm and W. M. Tang. Properties of ion temperature gradient drift instabilities in H-mode plasmas. *Physics of Fluids B: Plasma Physics*, 1(6):1185, 1989.
- [18] F. Romanelli. Ion temperature-gradient-driven modes and anomalous ion transport in tokamaks. *Physics of Fluids B: Plasma Physics*, 1(5):1018, 1989.

- [19] G. G. Plunk, P. Helander, P. Xanthopoulos, and J. W. Connor. Collisionless microinstabilities in stellarators. III. the ion-temperature-gradient mode. *Physics of Plasmas*, 21(3):032112, 2014.
- [20] M. N.A. Beurskens, S. A. Bozhakov, O. Ford, P. Xanthopoulos, A. Zocco, et al. Ion temperature clamping in Wendelstein 7-X electron cyclotron heated plasmas. *Nuclear Fusion*, 61(11):116072, 2021.
- [21] F. Ryter, C. Angioni, M. Dunne, R. Fischer, B. Kurzan, et al. Heat transport driven by the ion temperature gradient and electron temperature gradient instabilities in ASDEX Upgrade H-modes. *Nuclear Fusion*, 59(9):096052, 2019.
- [22] E. Fable, C. Angioni, and O. Sauter. The role of ion and electron electrostatic turbulence in characterizing stationary particle transport in the core of tokamak plasmas. *Plasma Physics and Controlled Fusion*, 52(1):015007, 2009.
- [23] J. H.E. Proll, H. E. Mynick, P. Xanthopoulos, S. A. Lazerson, and B. J. Faber. TEM turbulence optimisation in stellarators. *Plasma Physics and Controlled Fusion*, 58(1):014006, 2015.
- [24] J. Nührenberg and R. Zille. Quasi-helically symmetric toroidal stellarators. *Physics Letters A*, 129(2):113–117, 1988.
- [25] M. Landreman and E. Paul. Magnetic Fields with Precise Quasisymmetry for Plasma Confinement. *Physical Review Letters*, 128(3):035001, 2022.
- [26] A. H. Boozer. Plasma equilibrium with rational magnetic surfaces. *Physics of Fluids*, 24(11):1999, 1981.
- [27] M. Kotschenreuther, G. Rewoldt, and W. M. Tang. Comparison of initial value and eigenvalue codes for kinetic toroidal plasma instabilities. *Computer Physics Communications*, 88(2):128, 1995.
- [28] W. Dorland, F. Jenko, M. Kotschenreuther, and B. N. Rogers. Electron Temperature Gradient Turbulence. *Physical Review Letters*, 85(26):5579, 2000.
- [29] J. A. Baumgaertel, E. A. Belli, W. Dorland, W. Guttenfelder, G. W. Hammett, et al. Simulating gyrokinetic microinstabilities in stellarator geometry with GS2. *Physics of Plasmas*, 18(12):122301, 2011.
- [30] N. R. Mandell, W. Dorland, and M. Landreman. Laguerre-Hermite pseudo-spectral velocity formulation of gyrokinetics. *Journal of Plasma Physics*, 84(01):905840108, 2018.
- [31] N. R. Mandell, W. Dorland, I. Abel, R. Gaur, P. Kim, et al. GX: a GPU-native gyrokinetic turbulence code for tokamak and stellarator design. *arXiv preprint*, arXiv:2209, 2022.
- [32] M. Landreman and W. Sengupta. Constructing stellarators with quasisymmetry to high order. *Journal of Plasma Physics*, 85(6):815850601, 2019.
- [33] A. M. Dimits, G. Bateman, M. A. Beer, B. I. Cohen, W. Dorland, et al. Comparisons and physics basis of tokamak transport models and turbulence simulations. *Physics of Plasmas*, 7(3):969, 2000.
- [34] R. Jorge and M. Landreman. Ion-temperature-gradient stability near the magnetic axis of quasisymmetric stellarators. *Plasma Physics and Controlled Fusion*, 63(7):074002, 2021.
- [35] A. Mariani, S. Brunner, J. Dominski, A. Merle, G. Merlo, et al. Identifying microturbulence regimes in a TCV discharge making use of physical constraints on particle and heat fluxes. *Physics of Plasmas*, 25(1):012313, 2018.
- [36] S. P. Hirshman and J. C. Whitson. Steepest-descent moment method for three-dimensional magnetohydrodynamic equilibria. *Physics of Fluids*, 26(12):3553, 1983.
- [37] R. L. Dewar and S. R. Hudson. Stellarator symmetry. *Physica D: Nonlinear Phenomena*, 112(1-2):275, 1998.
- [38] M. Landreman, B. Medasani, F. Wechsung, A. Giuliani, R. Jorge, et al. SIMSOPT: A flexible framework for stellarator optimization. *Journal of Open Source Software*, 6(65):3525, 2021.
- [39] Pauli Virtanen, Ralf Gommers, Travis E. Oliphant, Matt Haberland, Tyler Reddy, et al. SciPy 1.0: fundamental algorithms for scientific computing in Python. *Nature Methods* 2020 17:3, 17(3):261–272, 2020.
- [40] V. V. Nemov, S. V. Kasilov, W. Kernbichler, and M. F. Heyn. Evaluation of $1/v$ neoclassical transport in stellarators. *Physics of Plasmas*, 6(12):4622, 1999.
- [41] C. Beidler, G. Grieger, F. Herrnegger, E. Harmeyer, J. Kisslinger, et al. Physics and engineering design for Wendelstein VII-X. *Fusion Technology*, 17(1):148, 1990.
- [42] C. G. Albert, S. V. Kasilov, and W. Kernbichler. Accelerated methods for direct computation of fusion alpha particle losses within stellarator optimization. *Journal of Plasma Physics*, 86(2):815860201, 2020.
- [43] A. Bader, M. Drevlak, D. T. Anderson, B. J. Faber, C. C. Hegna, et al. Stellarator equilibria with reactor relevant energetic particle losses. *Journal of Plasma Physics*, 85(5):905850508, 2019.